Acta
Materia
Medica

Research Article

Single-cell RNA sequencing reveals the effects of hederasaponin C in the treatment of diabetic nephropathy

Graphical abstract

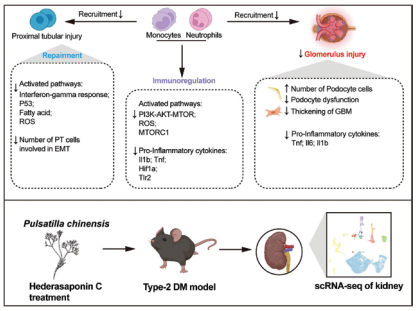

Highlights

- Integrated scRNA-seq and proteomics reveals gene expression changes during DKD and under PB5 treatment.
- DKD-induced injury in kidney epithelial cells was regulated by PB5 treatment.
- Intraglomerular ligand-receptor signaling at single-cell resolution.
- PB5 mediates the anti-inflammatory response in myeloid cells.

Authors

Jing Liu, Qian Zhang, Wentong Zhao, Jinan Guo, Yin Kwan Wong, Chunting Zhang, Weijin Qiu, Piao Luo, Junhui Chen, Junmao Li, Xiaoran Li, Hongwei Gao, Shilin Yang, Yulin Feng and Jigang Wang

Correspondence

jgwang@icmm.ac.cn (J. Wang);
fengyulin2003@126.com (Y. Feng)

In brief

Analyzing the impact of PB5 on mouse diabetic models using single-cell sequencing and proteomics reveals kidney cellular heterogeneity and transcriptional responses to DKD and PB5 treatment.

https://doi.org/10.15212/AMM-2023-0031
Acta Materia Medica 2023, Volume 2, Issue 4, p. 449-465

Acta Materia Medica

Research Article

Single-cell RNA sequencing reveals the effects of hederasaponin C in the treatment of diabetic nephropathy

Jing Liu[a,b,1], Qian Zhang[b,c,1], Wentong Zhao[a,1], Jinan Guo[b,1], Yin Kwan Wong[b,1], Chunting Zhang[d,e], Weijin Qiu[b], Piao Luo[c], Junhui Chen[b], Junmao Li[a], Xiaoran Li[a], Hongwei Gao[d,e], Shilin Yang[a], Yulin Feng[a,*] and Jigang Wang[a,b,c,f,*]

[a]National Pharmaceutical Engineering Center for Solid Preparation of Chinese Herbal Medicine, Jiangxi University of Chinese Medicine, Nanchang 330006, Jiangxi, China
[b]Department of Urology, Shenzhen Key Laboratory of Kidney Diseases, and Shenzhen Clinical Research Centre for Geriatrics, Shenzhen People's Hospital, The First Affiliated Hospital, Southern University of Science and Technology, Shenzhen 518020, Guangdong, China
[c]School of Traditional Chinese Medicine and School of Pharmaceutical Sciences, Southern Medical University, Guangzhou 510515, Guangdong, China
[d]College of Pharmacy, Guangxi University of Chinese Medicine, Nanning 530000, China
[e]Guangxi Engineering Technology Research Center of Advantage Chinese Patent Drug and Ethnic Drug Development, Nanning 530020, Guangxi, China
[f]State Key Laboratory for Quality Ensurance and Sustainable Use of Dao-di Herbs, Artemisinin Research Center, and Institute of Chinese Materia Medica, China Academy of Chinese Medical Sciences, Beijing 100700, Beijing, China

[1]These authors made equal contributions to this work.

***Correspondence:** jgwang@icmm.ac.cn (J. Wang); fengyulin2003@126.com (Y. Feng)

Received: 9 August 2023; Revised: 24 October 2023; Accepted: 30 October 2023

Published online: 21 December 2023

DOI 10.15212/AMM-2023-0031

ABSTRACT

There is great demand for the development of novel efficient therapeutic strategies or preventative measures to alleviate the life-threatening complications of type 2 diabetes. Hederasaponin C (PB5), a natural product, has been reported to exhibit significant therapeutic effects in various diseases; however, the possible effects and mechanism underlying PB5 in reducing diabetic renal complications have not been comprehensively reported. Here, we investigated the response of murine diabetic models to PB5 treatment using single-cell RNA-sequencing (scRNA-seq) and proteomics. Our findings revealed the dynamic transcriptional changes of renal cells in response to diabetic nephropathy. PB5 alleviated inflammatory injury by partially reducing pathophysiologic processes. In addition, we observed severe glomerular lesions and functional deficiencies, including GBM thickening and podocyte dysfunction, during the progression of diabetes, which were likewise attenuated by PB5. These results provide insight into how PB5 treatment improves diabetic symptoms and possibly serves as a novel protective measure and therapeutic strategy in the treatment of type 2 diabetes.

Keywords: type 2 diabetes, anti-inflammation, natural products, scRNA-seq, PB5

1. INTRODUCTION

Diabetic kidney disease (DKD) is the major cause of end-stage kidney disease (ESKD), affecting at least 20% of patients with diabetes [1]. DKD continues to be a prominent long-term complication of type 2 diabetes mellitus (T2DM) in association with insulin resistance (IR). There is mounting evidence supporting the involvement of oxidative stress, inflammation, and tissue fibrosis as key contributors to DKD progression, all of which impair glomerular filtration and cause damage to the endothelium and tubulointerstitium [2-5]. The kidneys, which have approximately 1 million functional units (nephrons), are susceptible to damage and infection resulting from high metabolic activity and hyperglycemia-induced immune dysfunction in diabetic individuals [6]. Despite recent advances in treatment, only modest reductions have been achieved in ESKD rates [7, 8].

Natural products are widely considered in drug discovery for diabetic treatment due to the reduced risk

Acta Materia Medica

of undesirable side effects, such as fluid retention and hypoglycemia, compared to other drugs [9-12]. Using single-cell technology in pharmacologic research involving natural products for diseases has enhanced our understanding of the mechanisms of actions for these compounds [13]. Hederasaponin C (PB5) is among the representative components of triterpenoid saponins extracted from the roots of *Pulsatilla chinensis*. PB5 has been reported to exhibit antioxidant and anti-inflammatory pharmacologic activities. Multiple studies have been conducted to explore the therapeutic potential of PB5 in various diseases, including schistosomiasis [14], acute lung injury [ALI] [15], and colitis. PB5 alleviates inflammation in rats with colitis by releasing pro-inflammatory cytokines, such as tumor necrosis factor (TNF), interleukin-1beta (IL-1β), and interleukin-6 [IL-6] [16]. However, the mechanism underlying PB5 in the treatment of DKD remains elusive, especially at the single cell level.

In the current study we combined single-cell RNA-sequencing (scRNA-seq) with proteomics technology to decipher the cellular events during diabetic progression and PB5 treatment by analyzing gene expression patterns and identifying related pathways. Our results provide comprehensive insight into treating diabetic nephropathy with PB5 by alleviating DKD-induced inflammation, epithelial injury, and fibrogenesis.

2. MATERIALS AND METHODS

2.1 Animal experiments

Eight-week-old male C57BLKS/J (45 ± 5 g [db/db mice]) and C57BL/6 mice (22 ± 2 g [healthy mice]) were obtained from Ji-Cui Pharma Biotechnology Co., Ltd. (Guangdong, China). The db/db mice, characterized by a deficiency in the leptin receptor gene, serve as a spontaneous mutation-based model for type 2 diabetes. The mice were maintained in standard laboratory facilities with an ordinary temperature (22 – 24°C) and 12-hour light/dark cycles. After feeding for 1 week, 8 male db/db model mice were randomly divided into 4 groups, including one model and 3 treatment groups (2 mice per group). The model group was administered saline buffer; the treatment groups were administered 300 mg/kg/d of metformin (MET; Sino-US Squibb Pharmaceutical Co., Ltd., Shanghai, China), or 20 or 40 mg/kg/d of PB5 for 39 days. Two healthy mice received saline buffer administration at the same time. The dosage was based on weight (0.01 ml/10 g). The body weight of each mouse was measured weekly and blood samples were obtained for measurement and analysis of physiologic indicators. The albumin-to-creatinine ratio (ACR) was determined in collected urine samples. Mice were anesthetized and sacrificed at the end of the experiments and kidney tissues were collected for use in scRNA-seq and histologic analysis.

2.2 Biochemical and histological analysis

Various indicators were tested, including blood urea nitrogen (BUN), creatinine (CRE), aspartate aminotransferase (AST), and alanine aminotransferase (ALT), using a Toshiba biochemistry instrument (TBA-120FR, Tokyo, Japan). A portion of the kidney tissues was embedded into paraffin, followed by cutting into sections for hematoxylin-eosin (H/E) staining. Masson's trichrome staining was used to confirm histologic morphology changes and the extent of fibrogenesis. Images were captured by microscopy.

2.3 Single cell suspension

Renal samples were chopped and enzymatically digested using the Multi Tissue Dissociation Kit-2 (Miltenyi Biotec, Bergisch Gladbach, Germany) on a MACS dissociator (Miltenyi Biotec, Bergisch Gladbach, Germany). The dissociated single cell solution was passed through a strainer (BD Biosciences, San Jose, USA) in PBS, then pelleted by centrifugation at 300 × g for 10 min at 4°C. Red blood cells were removed using Red Blood Cell Lysis Solution (Miltenyi Biotec). The cell pellets were resuspended in PBS sorting buffer after washing twice with PBS as a single cell suspension.

2.4 scRNA-seq data processing and cell type assignments

scRNA-seq libraries were established using the Chromium Next GEM Single Cell 3'Kit (v3.1; 10× Genomics, California, USA) according to the manufacturer's guidelines. The purified libraries were sequenced on the Illumina Nova-seq6000 platform (San Diego, California, USA) with 150bp paired-end reads. Raw sequencing data from each sample were demultiplexed and quality control was performed. The gene expression matrices obtained by Cell-Ranger (v6.0.1; 10× Genomics, California, USA) were aligned with mouse reference genome (mm10) for further analysis using the Seurat package (v4.0.4; New York, USA) of R software [17]. We then scaled and normalized the data across samples using the Seurat SCTransform function. The processed data were integrated and clustered at a proper resolution after principal components analysis (PCA) dimensionality reduction. Single cells were visualized in a two-dimensional uniform manifold approximation and projection (UMAP) space.

The Seurat FindAllMarkers function was applied to identify cell-specific markers for each cell cluster. These clusters were then identified and assigned to the corresponding types according to the expression of canonical markers, such as *Ptprc* for immune cells. In addition, cell subtypes were processed as described above, including PCA, clustering, and annotation. The model scores were inferred by the Seurat AddModuleScore function by calculating the average expression of predefined gene sets.

2.5 Differentially-expressed gene (DEG) analysis and functional enrichment

DEG between two comparisons (DKD/wild type [WT] and DKD/PB5) were generated using the Seurat FindMarkers function based on a filtered threshold (minimum percentage = 0.25; *P*-value < 0.05, $|\log_2$ fold-change$| \geq 0.25$). DEGs were further analyzed by gene ontology (GO) and the Kyoto Encyclopedia of Genes and Genomes (KEGG) using the clusterProfiler R package [v 3.18.1] [18]. The significant biological processes (BPs) with adjusted *P*-values from Benjamini-Hochberg multiple testing were selected for visualization. Gene set variation analysis (GSVA, v1.38.2; UPF, Barcelona, Spain) was used to assess the activation of pathways based on MSigDB Hallmark gene sets [19]. The differential pathways with an adjusted *P*-value < 0.05 were identified using the limma [20] R package (v3.48.3).

2.6 Trajectory analysis

We performed cell trajectory analysis on tubular epithelial cells with monocle2 R package (v2.20.0) to reveal cell state transitions [21]. GeneTest function was used to identify the differential cell states characterized by significantly altered genes. Finally, cell ordering and visualization were performed with the orderCells and plot_cell_trajectory functions.

2.7 Cellular communication analysis

CellChat (v2.0.0) was performed for cell-cell communication analysis with the default parameters based on the ligand-receptor interactions in different cell types. The meta information from normalized expression of gene and major cell types across groups served as the input for CellChat. The compareInteraction function was then performed to calculate interactive numbers among the three groups. For the distinctly changed cell populations, we then explored the ligand-receptor pairs between two comparisons and visualized the results as a bubble plot with the netVisual_bubble function.

2.8 Immunofluorescence analysis

Immunofluorescence staining was performed on cryosections of kidney tissues. The blocked tissues were cut into ~4 μm-thick sections after dewaxing and dehydration, then incubated with antibodies against α-SMA (14395-1-AP; Proteintech, Wuhan, China) and TNF-α (60291-1-Ig; Proteintech) and secondary fluorescent antibodies (Abcam, Cambridge, UK) overnight at 4 °C. The sections were mounted with Hoechst or 4′,6-diamidino-2-phenylindole (DAPI), and observed with a fluorescence microscope.

2.9 Western blot

Western blot was performed on kidney tissue proteins obtained using RIPA buffer (Beyotime, Shanghai, China) containing protease inhibitors. Equivalent amounts of proteins were separated using SDS-PAGE. Primary antibodies, including anti-IL-1β (16806-1-AP; Proteintech), anti-pan-Akt [Cell Signaling Technology (CST), USA], anti-phospho-Akt (Thr308; CST, USA), and secondary antibodies, were incubated for protein detection. The protein bands were quantified using the ImageJ system.

2.10 Label-free proteomics analysis

Proteomics data obtained by liquid chromatography-tandem mass spectrometry (LC-MS/MS) were subjected to differential analysis and visualization with R package. The limma R package was executed on proteins for identifying differentially-expressed proteins (DEPs) with an adjusted *P*-value < 0.05 and a fold-change ≥1.5. Next, the clusterProfiler R package was used for GO enrichment analysis of DEPs. The results were visualized via R package pheatmap and Cytoscape [22].

2.11 Statistical analysis

Non-scRNA-seq datasets in this study are presented as the mean ± standard deviation. One-way analysis of variance (ANOVA) was used to analyze the statistical differences across groups, unless otherwise mentioned. A *P*-value < 0.05 was considered statistically significant and indicated with asterisks (**P* < 0.05; ***P* < 0.01; ****P* < 0.001).

3. RESULTS

3.1 PB5 reduced DKD-induced kidney injury and dysfunction in mice

We used 8-week-old male C57BLKS db/db mice, which is a diabetic neuropathy model frequently used in animal studies [23-25] (**Figure 1a**). Age-matched healthy mice served as controls. After oral administration with saline, two concentrations of PB5 (20 or 40 mg/kg) or MET (300 mg/kg) for 39 d, assessment of vital signs showed that db/db model mice without any treatment developed more severe kidney hypertrophy and dysfunction, including proteinuria and an increased serum CRE level. We also observed histopathologic alterations, including increased glomerular area, thylakoid stroma proliferation, and vacuolar degeneration of the tubular epithelium when compared to WT mice based on H/E staining of renal tissues and evaluation of the renal injury degree by measuring the glomerular area (**Figures 1b, d and S1a, c**). These findings confirmed the occurrence of kidney impairment induced by diabetic nephropathy. In addition, immune-related or liver-function-related indicators, such as the percentage of lymphocytes (Lyms), white blood cell (WBC) count, percentage of neutrophils (NEUTs), and serum cholesterol (CHOL) and triglycerides (TG) concentrations were also remarkably increased in the db/db model mice compared to the WT group, while PB5 treatment significantly reversed these changes (**Figure S1c**). The effect of low-dose PB5 treatment (20 mg/kg) was better than PB5 (40 mg/kg; **Figure S1c**), as

Acta Materia Medica

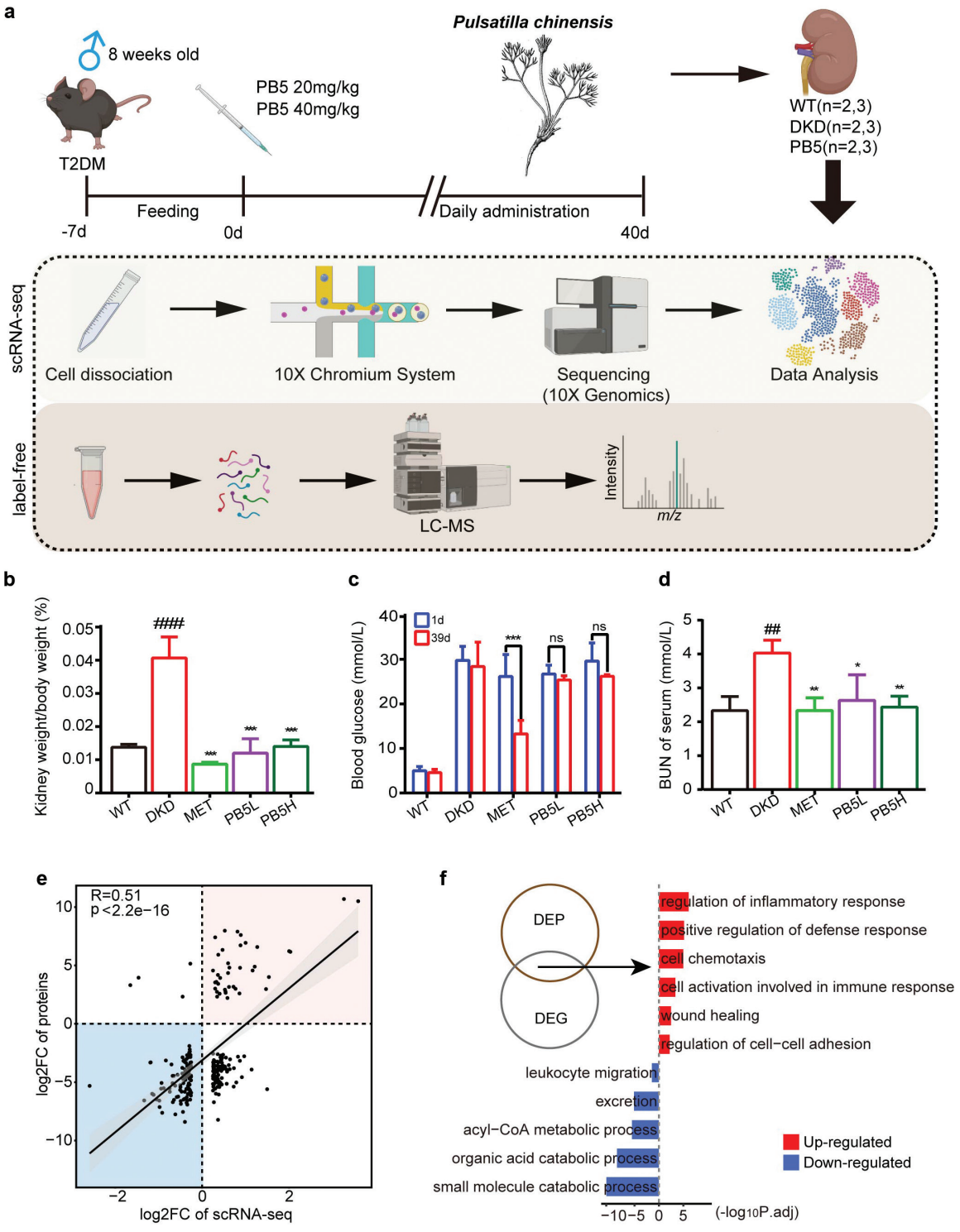

Figure 1 | Study design and physiologic readouts.

(a) The workflow of experimental strategy (n=2 mice per group for scRNA analysis; n=3 mice per group in mass spectrometry-based proteomics). (b) The ratio of kidney weight-to-body weight. (c) Blood glucose in experimental mice. (d) Blood urea nitrogen (BUN) in experimental mice. (e) Spearman's correlation of crossed DEGs ($|\log_2$ fold change$| > 0.25$, $P_{adjusted} < 0.05$) and DEPs expression ($|\log_2$ fold-change$| > 1.5$, $P_{adjusted} < 0.05$) between DKD versus WT and DKD versus PB5. Linear fitting is illustrated by a black line with confidence intervals (grey shading). Dots in the red and blue squares represent up- or down-regulated DEGs or DEPs, respectively. (f) GO enrichment analysis of overlaps between DEGs and DEPs in the diabetic group. $^{*}P < 0.05$, $^{**}P < 0.01$, $^{***}P < 0.001$ vs. DKD; $^{\#\#}P < 0.01$, $^{\#\#\#}P < 0.001$ vs. WT).

evidenced by alterations in the relative kidney weights and immune- or metabolic-related indices (percentage of NEUTs and low-density lipoprotein-cholesterol [LDL]).

To dissect the intracellular pathogenesis of diabetic nephropathy and assess the effects of PB5, we conducted scRNA-seq and MS on cryopreserved kidney tissues, which were obtained from WT mice, DKD mice, and mice treated with 20 mg/kg of PB5 (**Figures 1a and S2a**). We utilized three cohorts for scRNA-seq, each comprised of two renal tissue samples, and three cohorts for MS, each with three tissue samples. We identified 1131 DEPs and 4425 DEGs in the DKD group compared to the WT and PB5 groups (**Figures S2c and S4a**), with an overlap between the two sets (R = 0.51, P < 2.2e-16; **Figure 1e**). Consistent with kidney injury and dysfunction induced by diabetic nephropathy, GO analysis of the overlapping DEPs and DEGs demonstrated upregulation of pathways, including inflammatory response, defense or immune response, cell chemotaxis, and wound healing, while downregulated pathways included excretion and small molecule or organic acid catabolic processes (**Figures 1b-d, f and S1c**). We also enriched common up- or down-regulated DEGs between the DKD and other groups, and found activation of inflammatory responses, granulocyte migration, reactive oxygen species (ROS) metabolic processes, responses to oxidative stress, and intrinsic apoptotic signaling in the DKD group (**Figure S4b**). Moreover, immune cells, fibroblasts (Fibros), and endothelial cells (Endos) were prominently enriched in pathways associated with inflammatory responses, IL6-JAK-STAT3 signaling, and epithelial-mesenchymal transition (EMT; **Figure S4c**). Importantly, we also observed higher levels of inflammation-related gene expression enriched in immune cells (**Figure S4d**). These observations suggest that diabetes initiated inflammatory responses and oxidative stress in the kidneys, while PB5 treatment alleviated the recruitment of immune cells and the inflammatory response during DKD progression.

The protein abundance correlation between the DKD group and the other groups was weak based on MS-based proteomics data, indicating the unique DKD expression pattern and the effects of PB5 treatment on diabetic nephropathy (**Figure S2b**). We compared proteomics profiles from DKD to the WT and PB5 groups, and identified 132 and 377 common up- and down-regulated DEPs, respectively (**Figure S2d, e**). Interestingly, pathways involved in wound healing, regulation of inflammatory responses, innate immunity, oxidative stress, NF-kappaB signaling, and extracellular matrix organization were upregulated in the DKD group. We also found that pathways including the involvement of renal absorption, lipid homeostasis, and renal tubular secretion were downregulated in db/db mice (**Figure S2f**). By detecting the patterns of gene expression associated with upregulated inflammatory responses (*Anxa1*, *Adamts2*, *Il1b*, *Prtn3*, *C3*, and *Fgg*) or downregulated lipid metabolism signaling (*Ces1d*, *Ces1f*, and *Mlxipl*) in DKD mice, we further confirmed the anti-inflammatory effect of PB5 in diabetic nephropathy (**Figure S2g**). All gene patterns displayed the expected levels of expression, which were consistent with the protein profiles (**Figure S2f**). Fibrinogen gamma-chain (FGG) has been reported to be upregulated in the tubulointerstitium of patients with IgA nephropathy [26]. Therefore, we built up a protein-to-protein interaction (PPI) network for five proteins, including ANXA1, IL1B, PRTN3, C3, and FGG using the STRING database [27] (**Figure S2h**). Taken together, we found a high concordance between DEPs and DEGs in our study and identified the activation of pathways related to inflammatory responses, oxidative stress, and extracellular matrix organization, and metabolic dysregulation during the progression of DKD at the single-cell transcriptomic and proteomic levels.

3.2 Single-cell profiling of mouse kidneys in diabetic nephropathy and under PB5 treatment

To achieve a more comprehensive understanding of the molecular changes during diabetic pathology and PB5 treatment at a high resolution, we performed single-cell transcriptional sequencing on mouse kidney tissues across the three groups (WT, DKD, and PB5) using 10× Chromium technology (**Figure 1a**). We obtained a total of 26,344 single cells after quality control, including 8384 cells from WT mice, 9438 cells from DKD model mice, and 8522 cells from PB5-treated mice (**Figures 2a and S3a**). Based on UMAP analysis, the cells were categorized into clusters, which were comprised of cells derived from different biological replicates (**Figure 2d**), and further annotated into 12 major cell types based on canonical cellular markers, as follows: proximal tubular cells (PTs [n=17,903]) with high expression of *Slc27a2* and *Gatm*; podocytes (Podos [n=281]) with high expression of *Wt1* and *Nphrs2*; ascending loop of Henle (LOH [n=1218]) with high expression of *Slc12a1* and *Umod*; descending limb of loop of Henle (DTL [n=141]) with high expression of *Bst1* and *Aqp1*; distal convoluted tubule (DCT [n=1142]) with high expression of *Slc12a3* and *Pvalb*; connecting tubule (CNT [n=251]) with high expression of *Slc8a1* and *Dst*; collecting duct principal cells (CD-PCs [n=499]) with high expression of *Aqp2* and *Hsd11b2*; collecting duct intercalated cells (CD-ICs [n=286]) with high expression of *Atp6v1g3* and *Atp6v0d2*; Endos (n=1190) with high expression of *Flt1* and *Kdr*; Fibros (n=155) with high expression of *Tagln* and *Pdgfrb*; immune cells (n=3220) with high expression of *Ptprc*; and proliferative cells (Novels [n=58]) with high expression of *Mki67* and *Stmn1* (**Figure 2b**). Among these cell clusters, immune cells (*Ptprc*$^+$) were retained for further classification into Neutros, macrophages (Macros), B cells, and T cells by projecting the expression of signature markers on UMAP (**Figure S3c**).

Next, proportion analysis revealed a dramatic expansion in segments of PT cells compared with WT mice (**Figure 2c and e**), consistent with the increased

Acta Materia Medica

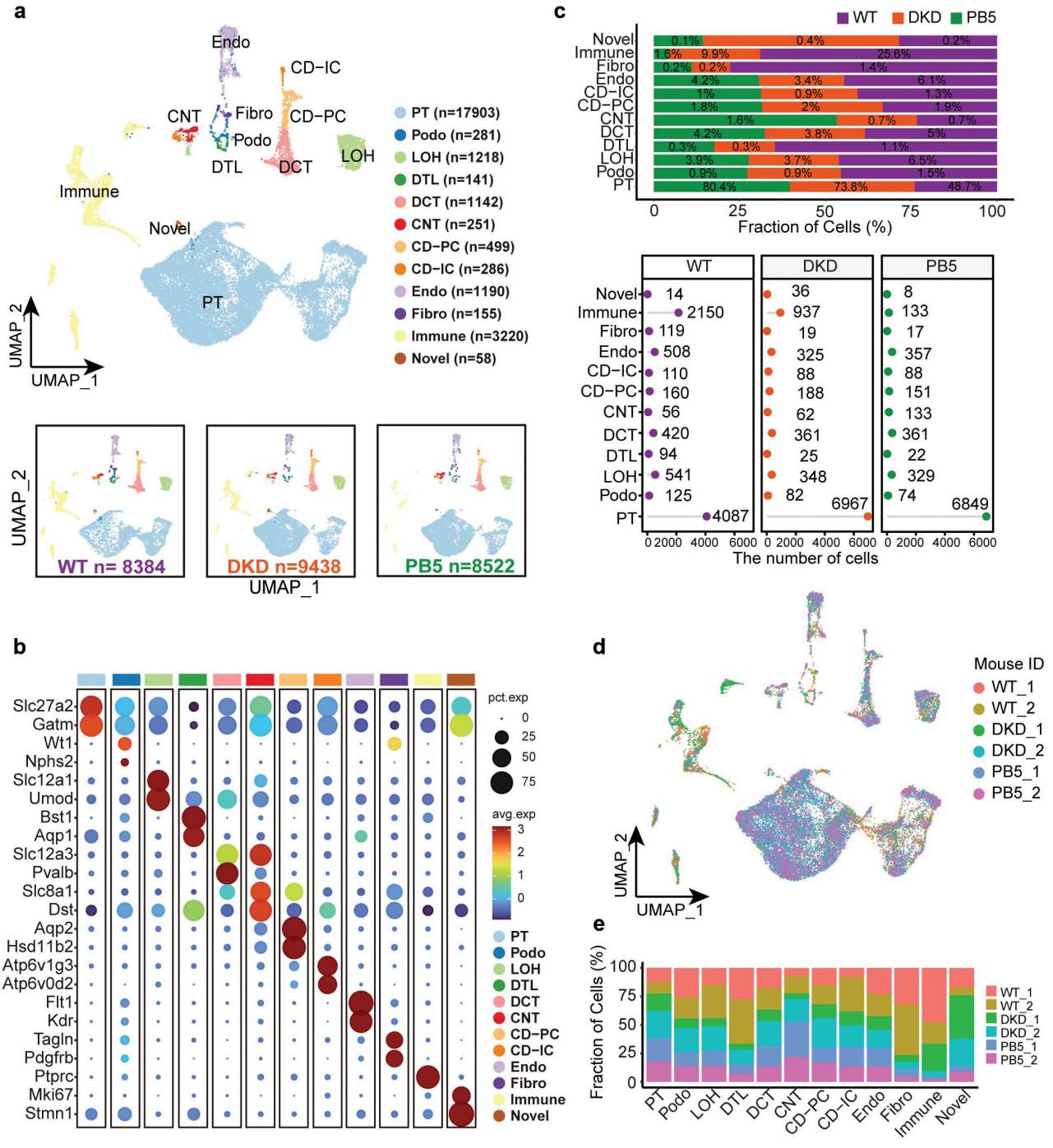

Figure 2 | Single-cell atlas of mouse diabetic kidney.
(a) UMAP plot of all integrated datasets from all mouse kidneys. (b) Dot plot showing the expression patterns of marker genes in each cell type. (c) Bar graph displaying the proportion of renal cells from each group (top) and cell numbers of all cell types in each group (bottom). (d) UMAP plot showing renal cells of each individual mouse. (e) Bar plot showing the composition of cell types in each sample.

abundance of PT cells occurring during the progression of diabetic nephropathy [28]. In contrast to PT cells, various segments exhibited diverse changes in proportion following the progression of DKD.

3.3 PB5 alleviates DKD-induced injury in epithelial cells

PT cells with metabolic hyperactivity are susceptible to various insults and dysfunction [29]. To provide an

in-depth description of the dynamic alterations in PT cells across the three groups, we performed unsupervised clustering on 17,903 mouse PT cells across each group, further yielding and annotating 7 subclusters, including PT_S1-to-S6 and a repairing subpopulation PT_cycling (*Mki67*$^+$), based on segment-specific markers (**Figures 3a and S5a, c**). Among these groups, PT_S1 and PT_S2 cells (which were also the main DKD-target subclusters) displayed prevalent expression of the representative markers of the proximal convoluted tubule [PCT] (*Slc5a12*$^+$) and proximal straight tubule [PST] (*Slc13a3*$^+$; **Figure 3a**), respectively. Other PT cell subtypes, including PT_S5 and PT_S6, were also expressed ([*SPP1*, *Cst3*] and [*Prdx1*, *Aldob*], respectively). Peroxiredoxin 1 (*Prdx1*) has been reported to exacerbate AKI by promoting inflammation [30]. Decreased proportions of S1, S2, and S3 were observed in the DKD group, while the percentage of S5 and S6 significantly increased by nearly 2-fold compared to WT (**Figure 3b**). Notably, changes in both trends were partly recovered by PB5 treatment (**Figures 3b and S5b**). Moreover, the expression of impairment-related markers (*Lcn2*, *Fabp1*, *Clu*, and *Spp1*) were mainly upregulated in S4, S5, and PT_cycling compared with other subtypes, and downregulated in the PB5 group compared to DKD, suggesting the protective effect of PB5, which was supported by the decrease in the relative expression of SPP1 (**Figure 3c**).

To further investigate transcriptional differences in PT cells across the three groups, we compared DEGs between DKD versus WT and DKD versus PB5 (**Figure S5d, e**). We identified 139 shared DEGs in DKD, and found that 84 upregulated DEGs were enriched in specific pathways, such as lipid oxidation and oxidative phosphorylation, while 55 downregulated DKD DEGs were enriched in regulation of Endo migration, cellular glucose homeostasis, and organic acid transport (**Figure S5d**). Moreover, GSVA was performed to characterize the pathogenesis of DKD in PT cells, identifying pathways, such as the activated interferon-gamma (IFN-γ) response, IL6-JAK-STAT3 signaling, and reactive oxygen species in DKD (**Figure S5e**). Abnormal ROS levels have been reported to be a contributing factor in the development of kidney fibrogenesis and injury [31]. In performing correlation analysis of the seven subclusters, all of the PT segments were clustered into 3 functional categories (C1–C3) with similar intraclass gene expression patterns (**Figure 3d**). Notably, higher scores related to the IFN-γ response and wound repair to inflammatory response were primarily observed in the DKD group among the 3 clusters, as analyzed using the Seurat package (detailed in the Methods section), indicative of the responses of PT cells to inflammation during DKD (**Figure 3d**).

To explore the lineage transitions of PT cells, as analyzed by Monocle2 (detailed in the Methods section), we built up a pseudo-time trajectory of these subclusters with a specific distribution, coinciding with the gene expression pattern between each subcluster or location of the UMAP plot (**Figure 3a, d-f**). We showed that the cells in PT_S1/S2 were prevalent in the initial phase of the renal system process, lipid homeostasis, and oxidative phosphorylation pathway (**Figure 3f**), while the cells in S5/S6 were mainly accumulated at the end of the path with activation of wound healing, cell-matrix adhesion, and EMT. These findings prompted us to assess the expression of ROS- and impairment-related genes. Elevated expression of impairment-related genes (*Spp1* and *Cst3*) and an ROS-related gene (*Hif1a*) were detected in S5/S6 (**Figure 3g**). In addition, based on regulatory network analysis [32], we detected 10 transcription factors in PT cells (**Figure 3h**). The activity score of *Ybx1* (YBX1), which is associated with regulation of the EMT [33] was upregulated in DKD (**Figure 3h**).

Next, we investigated the extent to which PB5 improved the response to diabetes-induced impairments in other epithelial segments, which consist of 6 cell types, including LOH, DTL, DCT, CNT, CD-PCs, and CD-ICs (**Figure 4a**). These epithelial segments were characterized by cell-specific marker genes and we observed the various abundances in these subclusters by comparing the proportion of cells in the DKD group to each other group (**Figure 4b, c**). To explore the transcriptional characteristics, we performed DEG analysis comparing DKD samples with the other groups (DKD vs. WT and DKD vs. PB5), as well as further GO enrichment analysis of the epithelial cells. Comparing the enrichment signal between DKD and the other groups revealed that pathways involved in the response to oxidative stress were enriched in upregulated DEGs, while immune-related processes were downregulated (**Figure 4d**). Moreover, we observed significant diabetic nephropathy-induced injury and ROS changes in these nephron segments based on injury or ROS-related gene sets (**Figure 4e**). In addition, functional solute carriers involved in the regulation of renal reabsorption function, such as Slc22a12, Slc38a3, Slc7a12, Slc22a2, Slc34a3, Slc22a8, and Slc22a6, displayed the highest expression in PT cells compared with other epithelial, and the expression of these carriers were downregulated in the DKD group compared to the WT and PB5 groups (**Figure 4g**). Interestingly, the expression of the injury-related genes and these transmembrane transporters were also decreased in the DKD proteomics data. Collectively, these results indicate that renal epithelial cells were damaged and dysfunctional during DKD, while PB5 relieved the injury by alleviating the inflammatory response.

3.4 PB5 remodels the glomerular microenvironment during diabetic nephropathy

Recent single cell studies have demonstrated the complexity and heterogeneity of both normal and impaired stromal cells [34-36]. To characterize these cells in the context of our study, we re-clustered all of the stromal cells collected in our experiments into 6 clusters, according to the expression of marker genes reported by previous scRNA-seq studies [36, 37] (**Figure 5a**):

Acta Materia Medica

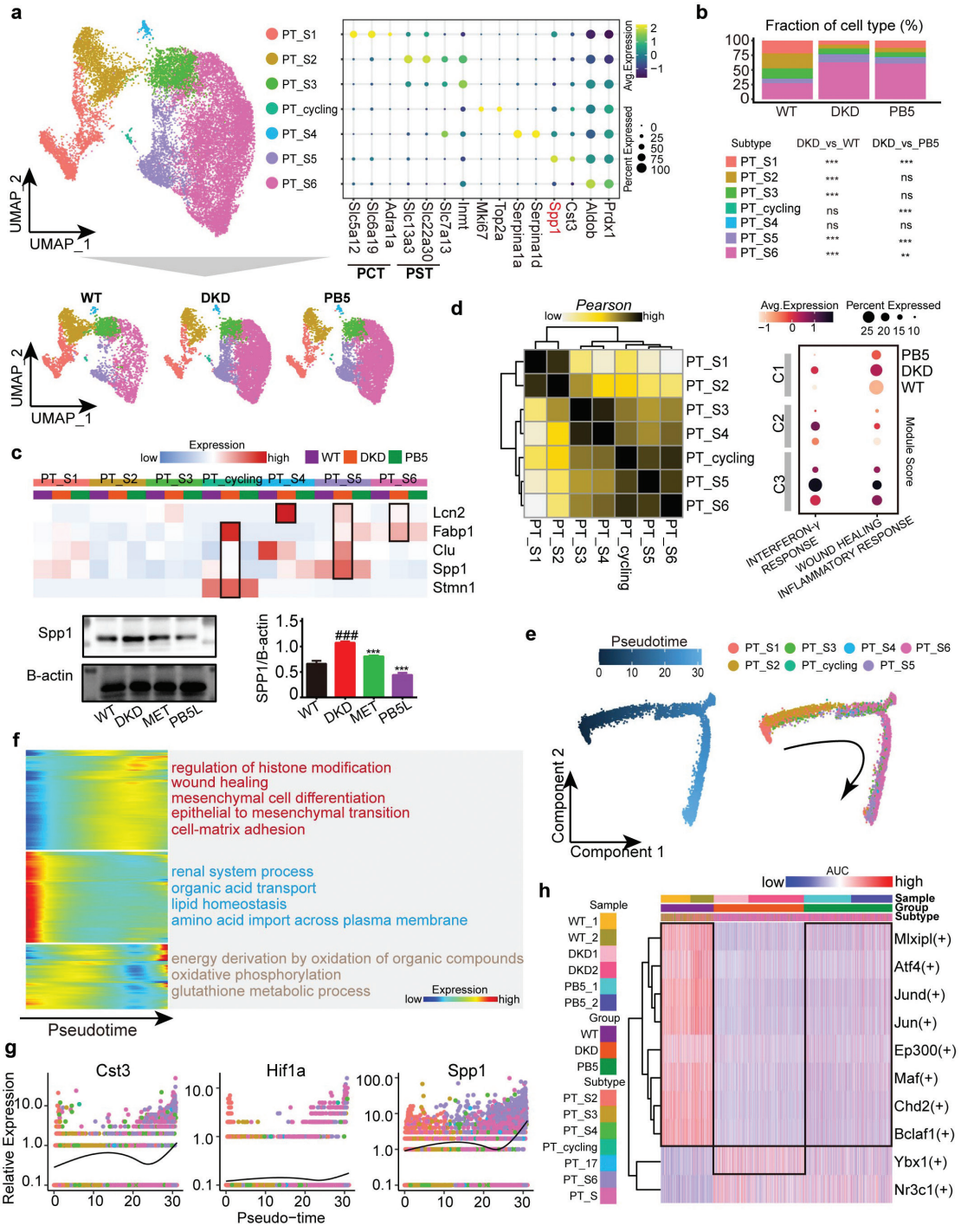

Figure 3 | Proximal tubular cell subtypes and the injury response to T2DM.
(a) UMAP plot showing unsupervised clustering (left) and the expression pattern of cell-specific markers (right), indicating seven subtypes of PT cells. (b) Bar plot displaying the percentages of each subtype between the three groups. $^{**}P < 0.01$, $^{***}P < 0.001$, ns > 0.05. (c) Heatmap showing the expression of renal impairment-related genes in subtypes from all PT cells (top) and western blotting detection of Spp1 protein levels (bottom). $^{***}P < 0.001$ vs. DKD; $^{\#\#\#}P < 0.001$ vs. WT. (d) Heatmap showing correlation coefficients among subtypes of the three groups (left). Dot plot (right) showing enriched scores between the three groups for 3 classes (C1: PT_S1, PT_S2, PT_S3; C2: PT_S3, PT_S4; and C3: PT_cycling, PT_S5, PT_S6). (e) Pseudotime trajectory of PT cells colored by pseudo-time and subtypes. (f) Heatmap presenting the changes in relative gene expression along with the pseudotime and enriched upregulated biological processes (right). (g) Plot displaying the dynamic expression of injury and inflammatory genes along the pseudotime. (h) Heatmap showing the relative activity scores of the ten regulons in different samples, groups, and subtypes.

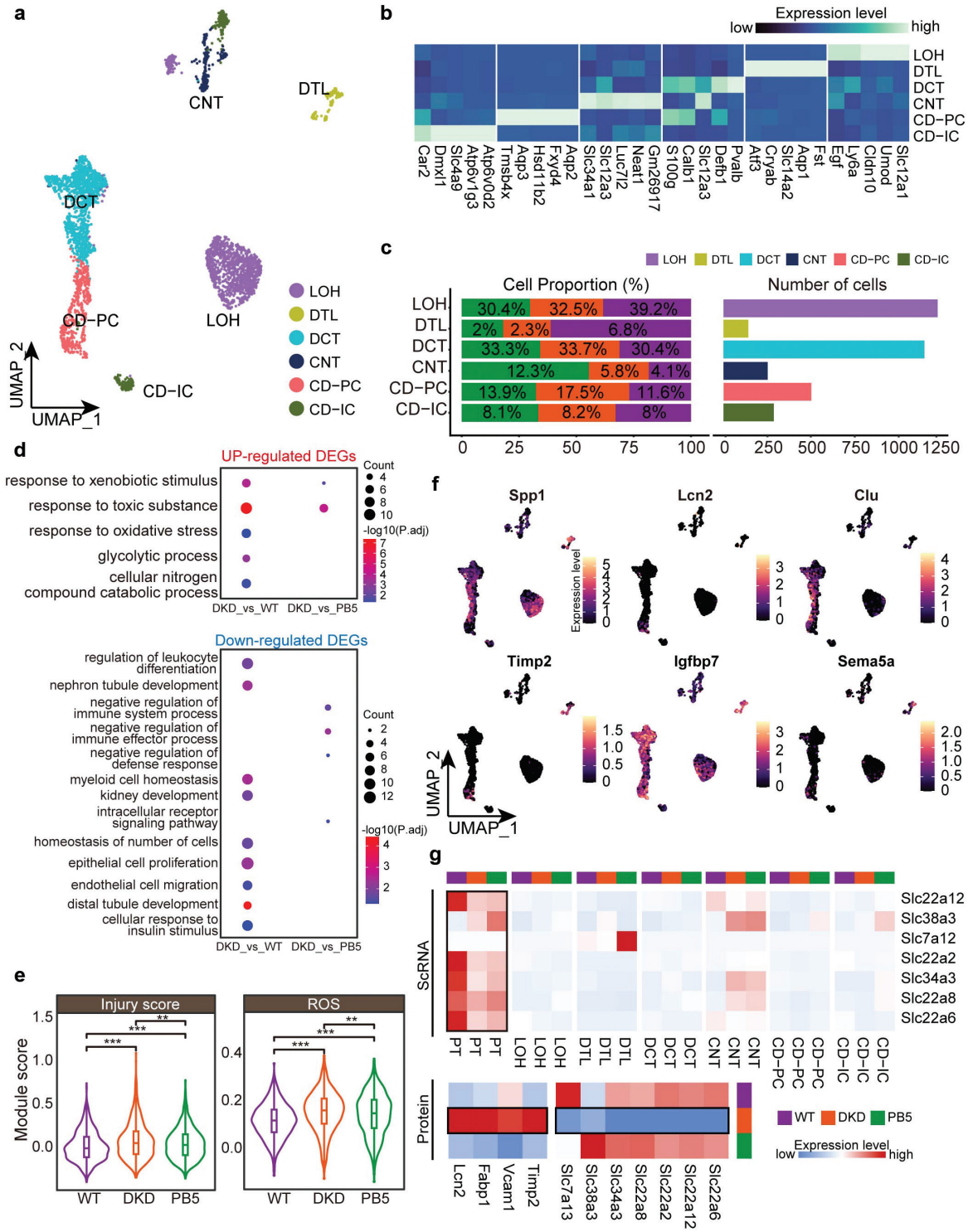

Figure 4 | Diabetes-induced injury response in nephron segments.
(a) UMAP plot showing the clustering. (b) Heatmap showing the expression pattern of cell-specific markers of the six epithelial cell types. (c) Bar graph displaying the proportion of epithelial cells from each group and cell number of individual cell types. (d) Bubble plot showing the GO enriched terms of up- and down-regulated DEGs between DKD versus WT and DKD versus PB5. (e) Violin plot showing the changes in enrichment scores with respect to injury and ROS in the three groups. (*P* values [Wilcoxon signed-rank test]). $^{**}P < 0.01$, $^{***}P < 0.001$. (f) UMAP plot showing the expression of cell-specific canonical markers in the integrated data. (g) Heatmap showing the expression of transporters in all epithelial cells across each group in the scRNA dataset (top) and proteomics dataset (bottom).

Acta Materia Medica

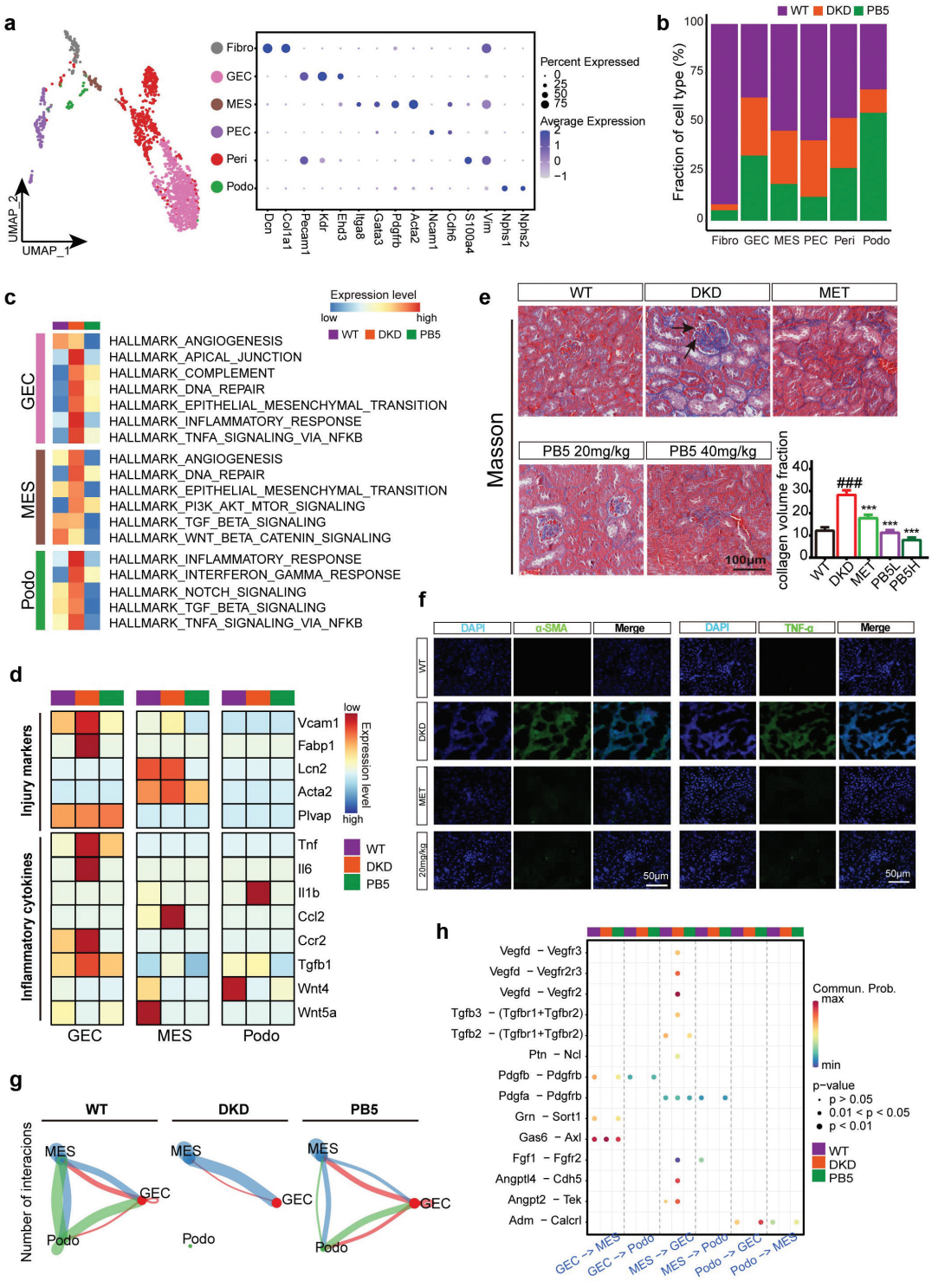

Figure 5 | Glomerular lesions and cellular interaction network across the three groups.
(a) UMAP plot displaying the reclustering of glomerular cells. Dot plot showing the expression patterns of marker genes in each cell type. (b) Bar graph displaying the proportion of glomerular cells by each subcluster. (c) Heatmap showing GSVA scores of glomerular cells in each type. (d) Heatmap showing the expression of specific marker genes in each group. (e) Masson's trichrome staining showing the changes in renal parenchyma in diabetes. $^{***}P < 0.001$ vs. DKD; $^{\#\#\#}P < 0.001$ vs. WT. (f) Immunofluorescence staining of DAPI (blue), α-SMA (green), and TNF-α (green) in renal tissues. Scale bar: 50 μm. (g) Communication network between GECs, MESs, and Podos in the three groups. (h) Bubble plot showing ligand-receptor pairs between GECs, MESs, and Podos.

Fibros (*Col1a1*$^+$*DCN*$^+$); glomerular endothelial cells [GECs] (*Pecam1*$^+$*Kdr*$^+$*Ehd3*$^+$); mesangial cells [MESs] (*Itga8*$^+$*Gata3*$^+$*Pdgfrb*$^+$); parietal epithelial cells [PECs] (*Ncam1*$^+$*Cdh6*$^+$); pericytes [Peris] (*S100a4*$^+$*Vim*$^+$); and podocytes [Podos] (*Nphs1*$^+$*Nphs2*$^+$). Among the clusters, smooth muscle alpha-actin *Acta2* (α-SMA), which is involved in the activation of fibrogenesis, was highly expressed in the MES subcluster (**Figure 5a**). In addition, GECs and Podos had a decreasing proportional trend in the DKD group compared to the WT group, while the fractions were reverted following PB5 intervention (**Figure 5b**). The glomerulus, responsible for kidney filtration, mainly consists of Endos, MESs, and Podos. The loss of glomerular function is the leading cause of pathogenesis in DKD. Moreover, factors, such as immune injury, contribute to glomerular dysfunction.

To further elucidate the glomerular-specific variations in DKD, we investigated Hallmark pathways between DKD/WT and DKD/PB5 across the three major glomerular subclusters (GEC, MES, and Podo). Pathways involved in inflammation response, including TNF-α signaling via NF-kB, angiogenesis, and EMT, were primarily enriched in diabetic mice, while WNT/β-catenin signaling was reduced in the DKD group (**Figure 5c**). As presented in **Figure 5d**, GEC cells had high expression of injury maker genes (*Vcam1*, *Fabp1*, and *Plvap*) and pro-inflammatory cytokines (*Tnf* and *Il6*) compared to the WT and PB5 groups, while *Acta2* was highly expressed in the DKD group for MES cells. In addition, the expression of TGFβ1, a main driver of fibrosis, was enriched in the DKD group and reversed after PB5 treatment. PB5 treatment also reduced the expression of monocyte chemokines and the receptor (Ccl2/Ccr2) in GECs and MES cells, and increased the expression of Wnt4 and Wnt5a (**Figure 5d**). As glomerular injury and activation of proinflammatory-related pathways are likely drivers of glomerulitis and fibrogenesis, we performed Masson staining to confirm the extent of impairment. As shown in **Figure 5e**, we observed hypertrophied glomeruli with discrete intra-globular stromal hyperplasia and magnified tubular lumens with naked cell nuclei. Moreover, immunofluorescence staining revealed that the levels of SYNPO and NPHS2 protein expression (indicative markers of Podos) were suppressed in diabetic mice, which could induce abnormal morphology and filtration function of Podos, such as in segmental glomerulosclerosis [38, 39]. In addition, we observed high levels of α-SMA and TNF-α expression in the DKD group, as representative markers of fibrogenesis and pro-inflammatory factors, which was consistent with the expression of *Acta2* and *Tnf* in **Figure 5d**. Importantly, the increased α-SMA and TNF-α expression in the DKD group was reversed, as expected, by PB5 treatment (**Figure 5f**). The effectiveness of PB5 treatment was further verified by the remarkable alleviation of fibrotic glomeruli and increased synthesis of key glomerular components, such as podocin and synapto-podin, to repair podocyte damage (**Figures 5e and S6a**).

Next, we analyzed the crosstalk between GECs, MESs, and Podos, and observed that the number of cellular interactions decreased in the diabetic model (especially in Podos), and again recovered after PB5 treatment, which was consistent with previous results (**Figure 5g**). Ligand-receptor pair analysis revealed that VEGF, ANGPTL4, and ADM signaling were significantly reduced by renal diabetes, with PB5 treatment reversing this reduction (**Figure 5h**).

Our profiles thus provide a detailed analysis of glomerular cells during DKD and PB5 treatment. These findings showed that PB5 relieved diabetes-induced glomerular inflammatory injury and fibrogenesis, thereby improving the proinflammatory tissue microenvironment and prompting kidney tissue repair.

3.5 PB5 alleviates the recruitment of monocytes and infiltration of Neutros

Myeloid cells are capable of self-replenishment following inflammation or injury and are responsible for the innate immune defense against toxins or pathogens [40]. Fibrotic renal damage is caused by vascular formation and inflammatory over-responses [41]. We classified 10 subpopulations in the myeloid lineages with unsupervised clustering, including two subclusters for monocytes [Monos] (Mono_C1 and Mono_C2), Neutros (Neutro_C1 and Neutro_C2), Macros (Macro_C1 and Macro_C2), and conventional dendritic cells (cDCs) (cDC1 and cDC2), and one subcluster each for plasmacytoid dendritic cells (*Runx2*$^+$, *Siglech*$^+$) and actively proliferating cells (*Mki67*$^+$, *Top2a*$^+$). Monocytes were defined as *CD14*$^+$*Ace*$^+$ and *CD14*$^+$*Ly6c2*$^+$*Chil3*$^+$ clusters. Macros were identified via high expression of the *C1qa*$^+$*C1qb*$^+$ markers. Macro_C1 expressed known M1 or M2 markers (*Cd86*$^+$, *Mcr1*$^+$, and *Cx3cr1*$^+$). Interestingly, cells in Neutro_C2 with the expression of chemokine-related genes (*Cxcl2*$^+$*Ccl3*$^+$*Cxcl3*$^+$) were observed predominantly in the diabetic mice group compared with the WT and PB5 groups (**Figures 6a, b and S7a**). For the comparison between each subcluster, the immune fraction revealed that the proportion of Macros was lower in the DKD group, whereas the proportion of Monos and Neutros were higher in DKD mice and remarkably reversed after PB5 treatment (**Figure 6b**).

Next, we analyzed the enriched pathways comparing DKD mice with each of the other groups and found that activated pathways involved in inflammation-related signaling were upregulated in diabetes, including the response to type I IFN, ROS metabolic processes, and leukocyte chemotaxis (**Figure 6c**). VEGF, PI3K-Akt, and NF-kappa B signaling, IR, and focal adhesions were prevalent in Mono_C1, while the pathway associated with cytokine-cytokine receptor interaction was enriched in Neutro_C2, and antigen processing and presentation was upregulated in Macro_C1 (**Figure S7b**). We further assessed inflammatory-related enrichment scores based on multiple gene sets (details in the Methods section), and these results indicated a heterogeneous response

Acta Materia Medica

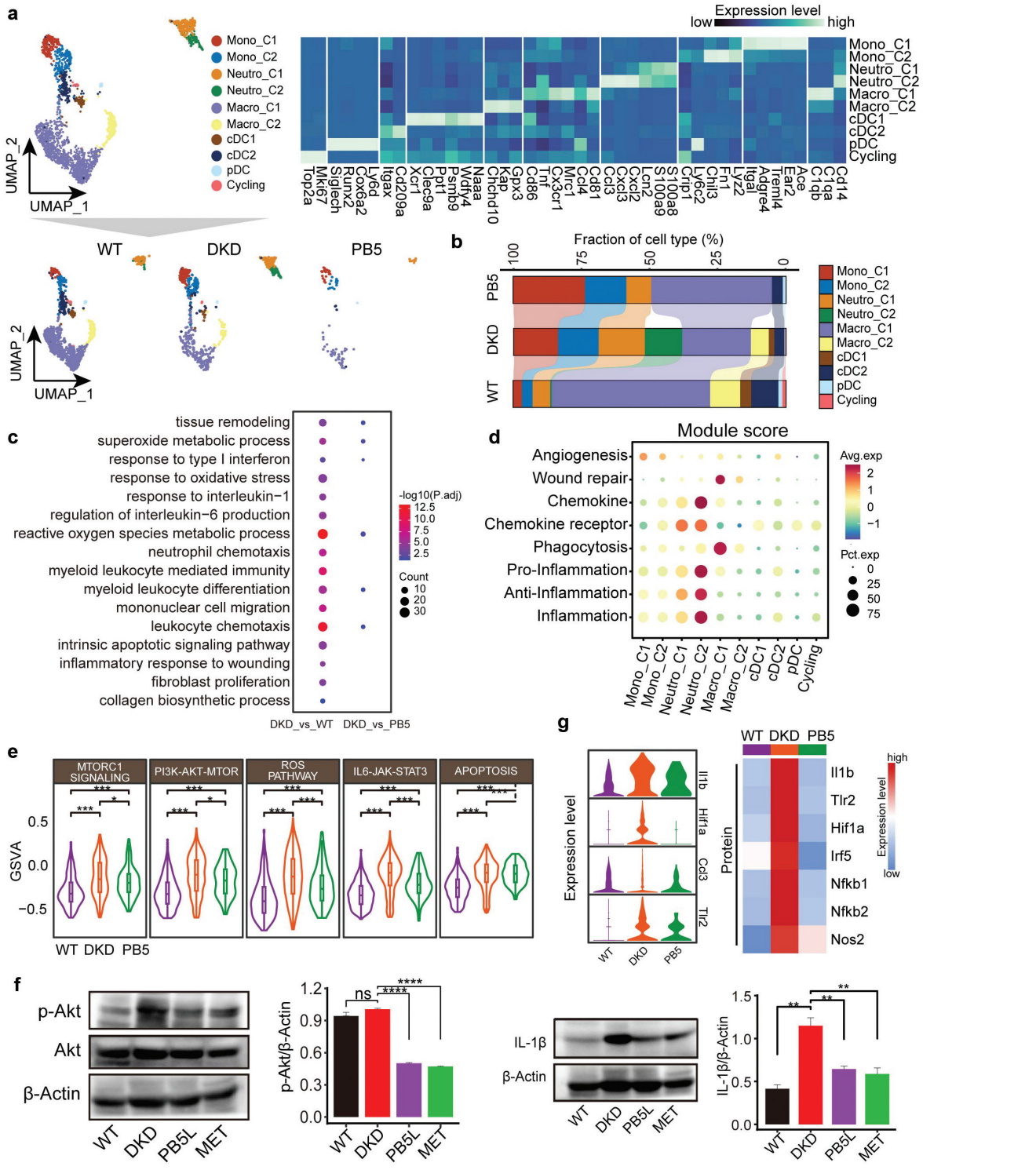

Figure 6 | Activated monocytes induce angiogenesis and inflammation in diabetes.
(a) UMAP visualization and cluster-specific gene expression in 10 myeloid subtypes. (b) Bar plot showing the composition of cell subtypes. (c) Bubble plot showing the GO enriched pathways in the two comparisons (DKD vs. WT and DKD vs. PB5). (d) Dot plot showing enriched scores of myeloid cells using 8 predefined gene sets. (e) Violin plot presenting the mTORC1, PI3K-Akt-mTOR, ROS, IL6-JAK-STAT3, and APOPTOSIS scores among the three groups based on GSVA analysis (***P*** values [Wilcoxon signed-rank test]). (f) Western blotting detection of p-Akt and Akt protein levels. **P* < 0.05, ***P* < 0.01, ****P* < 0.001; *****P* < 0.0001; ns > 0.05. (g) Violin plot displaying the relative expression levels of pro-inflammatory cytokines in the scRNA dataset (left) and proteomics dataset (right). Western blotting detection of IL-1β protein levels (bottom).

of renal myeloid cells (**Figure 6d**). Of those subclusters, monocytes had the highest angiogenesis score, which was compatible with the results shown in **Figure S7b**. Pathways involved in mTORC1, ROS, and PI3K-Akt-mTOR, which are associated with EMT [42], and Podo injury [43], were activated under diabetic progression (**Figure 6e, f**). We also confirmed the expression of the pro-inflammation cytokine, IL-1β, which was upregulated in the DKD group compared with the WT group and reversed after PB5 treatment and consistent with western blot results (**Figure 6g**) and with our proteomics data. To further delineate the dynamic transcriptomic changes involved in myeloid cells from diabetic cases, we performed GO analysis on the overlapped DEGs between DKD/WT and DKD/PB5 and identified an upregulation of the ROS pathway associated with the inflammatory response during diabetes (**Figure S7b**).

3.6 Cell-cell interactions during DKD and PB5 treatment

To verify cell-cell interactions and alterations during diabetes and PB5 treatment, we compared differential interactions among cell types and built up a group-centric ligand-receptor (LR) pairs profile between sender-receiver cells using CellChat [44]. We observed substantial changes in intercellular interactions induced by diabetes and hyperactive signaling mainly enriched in Endos, Fibros, and Podos (**Figure S6b, c**). We observed upregulated interactions comparing both DKD/WT and DKD/PB5 in Endos and Fibros acting as sender or receiver cells.

We further investigated the LR pairs and identified 18 pairs after filtering and selection. The PTN/SDC2/4 axis is actively involved in the regulation of renal function during diabetes through the secretion of multiple cytokines and hormones from the pituitary gland [45]. An increased possibly of PTN/NCL interaction between Fibros and Endos in the DKD group was likely to regulate angiogenic activities and promote PTN-induced Endo migration [46]. Our results suggest that diabetes significantly induced the activity of the fibroblast growth factor 1 (FGF1)/FGFR1 axis, which has been reported to be involved in thrombopoiesis, activating NF-κB, and metastasis through EMT [47-49]. We also observed an increase in the number of pathways between Fibros and Endos via VEGFD_VEGFR3, VEGFD_VEGFR2R3, and TGFB1/3_(TGFB1+TGFB2) in the DKD group. These signals were attenuated by PB5 treatment.

In summary, our analysis revealed several key crosstalk pathways between Endos and Fibros induced by diabetes, such as the PTN/NCL, FGF1/FGFR1, and TGFB1/3_(TGFB1+TGFB2) axis, while PB5 reverted these activations.

4. DISCUSSION

Our results identified the potential cellular mechanisms underlying T2DM and the protective ability of PB5 against inflammation and fibrosis. Diabetes is the principal factor contributing to chronic kidney diseases [CKDs] [50, 51]. The distinct pathologic features of DKD, such as kidney hypertrophy, have been reported to be linked to poor prognosis in type 1 and 2 diabetes [52, 53]. Changes, including proteinuria, hyperglycemia, and metabolic dysregulation of the liver, were also elaborated upon in this study. We performed scRNA-seq analysis on the kidney tissues of DKD mice to construct a cellular atlas and investigate the renal response during the progression of diabetes and PB5 treatment.

We observed activated pathways involved in ROS, inflammatory-related responses, wound repair, and EMT signaling in PTs induced by impaired renal epithelial cells, suggesting that these intrinsic changes stimulate the deposition of the extracellular matrix along with loss of kidney function [54], eventually leading to the development of interstitial fibrosis [55, 56]. In agreement with recent findings, renal tubular epithelial cells under kidney injury could be changed to a profibrotic phenotype [56]. The EMT, along with loss of epithelial characteristics and maladaptive repairment, stimulates the secretion of pro-inflammatory cytokines, apoptotic inhibition, or even deposition of the extracellular matrix [57, 58]. According to our proteomics analysis, we also found that the diabetic mice exhibited cell impairment caused by pro-inflammatory mediators and fibrosis-related pathways, which resulted in deposition of extracellular matrix in renal tissues [59]. PB5 regulated the activity of pro-inflammatory factors.

In addition, a previous report showed that injury to tubular epithelial cells facilitates the innate immune response, which is characterized by the activation and infiltration of circulating leukocytes, such as Monos and Neutros [60]. Bloodstream Monos migrate into the injured peripheral tissues, which contribute to promote Macro differentiation [61, 62]. During DKD, wound repair and phagocytosis functions were enhanced in the C1 cluster of Macros. C2 Monos, which are characterized by the expression of *Ccl2* (MCP-1), is a Mono chemokine and recruited in DKD mice consistent with Neutro_C2. Neutros are well-known for migration to injured tissues and chemotaxis [63, 64]. In addition, the pro-inflammatory microenvironment, which is characterized by activated ROS associated with EMT and the regulation of Akt/mTOR [42, 65-67] () and up-regulated expression of pro-inflammatory factors (*Il-1β* and *Hif1a*), were alleviated by PB5.

According to histologic staining and the results from scRNA-seq analysis, we confirmed the presence of glomerular lesions with GBM thickening and MES cell hyperplasia with a high level of *Acta2* expression in diabetic nephropathy. The LR analysis revealed enhanced interactions between MESs and GECs in the DKD group via the Vegfd/Vegfr2 axis involves angiogenesis [68], and the Tgfb2/(Tgfbr1+Tgfbr2) axis. TGFβ-2 acts as an immune suppressor in the intestines to reduce the secretion of inflammatory cytokines derived from Macros [69, 70]. Inhibition of TGFβ-2 alleviates the infiltration of Macros along with decreasing pro-inflammatory factors,

which could improve IR through paracrine effects [71]. The interaction of Tgfb1/(Tgfbr1+Tgfbr2) between Fibros and Endos were enhanced in the DKD group. TGFβ-1 signaling has been reported to be involved in inducing renal fibrosis or injury [72].

There were some limitations in our study. First, different cell types display variations in dissociation efficiency. We have only observed a small portion of Podos in all the clusters, which might be attributed to the fragility of the majority of Podos under the single cell dissociation process. In the future, advanced biotechnology can be used to minimize cell loss. Second, while we detected impaired epithelial cells induced by inflammation, the cellular network involved in regulation of epithelial injury was not detected.

5. CONCLUSION

In summary, our results offer a comprehensive analysis to describe the cellular mechanisms and physiologic changes involved in diabetes-induced renal lesions and fibrogenesis through scRNA-seq and proteomics. This study also demonstrated the protective role of PB5 against diabetes by alleviating inflammation and fibrogenesis during the progression of T2DM. Our findings highlight PB5 as a potential therapeutic agent for future translation in diabetes.

ABBREVIATIONS

DKD, diabetic kidney disease; PB5, hederasaponin C; scRNA-seq, single-cell RNA transcriptome sequencing; MES, mesangial cell; PEC, parietal epithelial cell; GEC, glomerular endothelial cell; Podo, podocytes; Peri, pericytes; T2DM, type 2 diabetes mellitus; IL-1β, interleukin-1beta; TNF-α, tumor necrosis factor-alpha; EMT, epithelial-mesenchymal transition; ALI, acute lung injury; IR, insulin resistance; CCL2, motif chemokine ligand 2; BUN, blood urea nitrogen; ACR, the ratio of urinary albumin-to-creatinine; CRE, creatinine; TG, triglycerides; LDL, low-density lipoprotein cholesterol; CHOL, cholesterol; WBC, white blood cell; Lym, lymphocyte; AST, aspartate aminotransferase; UMAP, uniform manifold approximation and projection; PCA, principal components analysis; DEG, differentially-expressed gene; DEP, differentially-expressed protein; GO, gene ontology; KEGG, Kyoto Encyclopedia of Genes and Genomes; GSVA, gene set variation analysis; Neutro, neutrophil; NF-κB, nuclear factor kappa-B; GSA, genome sequence archive; ECM, extracellular matrix; PT, proximal tubule; PST, proximal straight tubule; PCT, proximal convoluted tubule; WT, wild type; MET, metformin; DCT, distal convoluted tubule; DTL, descending limb of loop of Henle; Endo, endothelial cells; Fibro, fibroblasts; Macro, macrophages; CNT, connecting tubule; CD-IC, collecting duct intercalated cell; CD-PC, collecting duct principal cell; LOH, ascending loop of Henle; GEC, glomerular endothelial cells; GBM, glomerular basement membrane; H/E, hematoxylin and eosin.

ACKNOWLEDGEMENTS

The study was supported by the Establishment of Sino-Austria "Belt and Road" Joint Laboratory on Traditional Chinese Medicine for Severe Infectious Diseases and Joint Research (2020YFE0205100), Jiangxi University of Chinese Medicine Science and Technology Innovation Team Development Program [CXTD22001], the Distinguished Expert Project of Sichuan Province Tianfu Scholar (CW202002), the Fundamental Research Funds for the Central public welfare research institutes (ZZ13-ZD-07), Shenzhen Clinical Medical Research Center for Geriatric Diseases, the Science and Technology Foundation of Shenzhen (JCYJ20210324115800001), the National Key Research and Development Program of China (2020YFA0908000 and 2022YFC2303600), the Shenzhen Science and Technology Innovation Commission (JCYJ20200109120205924 and RCYX20221008092950121), the Innovation Team and Talents Cultivation Program of National Administration of Traditional Chinese Medicine (ZYYCXTD-C-202002), the Shenzhen Key Medical Discipline Construction Fund (SZXK046), The Shenzhen Medical Research Fund of Shenzhen Medical Academy of Research and Translation (B2302051) CACMS Innovation Fund (CI2023E002), and the National Natural Science Foundation of China [82074098 and 81841001].

CONFLICT OF INTEREST

The authors declare no conflicts of interest.

REFERENCES

[1] Hakim FA, Pflueger A: Role of Oxidative Stress in Diabetic Kidney Disease. *Medical Science Monitor Basic Research* 2010, 16:RA37– RA48.
[2] Fu J, Sun Z, Wang X, Zhang T, Yuan W, Salem F, et al.: The Single-Cell Landscape of Kidney Immune Cells Reveals Transcriptional Heterogeneity in Early Diabetic Kidney Disease. *Kidney International* 2022, 102:1291–1304.
[3] Ricciardi CA, Gnudi L: Kidney Disease in Diabetes: From Mechanisms to Clinical Presentation and Treatment Strategies. *Metabolism* 2021, 124:154890.
[4] Pan J, Zhou L, Zhang C, Xu Q, Sun Y: Targeting Protein Phosphatases for the Treatment of Inflammation-Related Diseases: From Signaling to Therapy. *Signal Transduction and Targeted Therapy* 2022, 7:177.
[5] Winiarska A, Knysak M, Nabrdalik K, Gumprecht J, Stompór T: Inflammation and Oxidative Stress in Diabetic Kidney Disease: The Targets for SGLT2 Inhibitors and GLP-1 Receptor Agonists. *International Journal of Molecular Sciences* 2021, 22:10822.
[6] Berbudi A, Rahmadika N, Tjahjadi AI, Ruslami R: Type 2 Diabetes and its Impact on the Immune System. *Current Diabetes Reviews* 2020, 16:442–449.
[7] Perkovic V, Jardine MJ, Neal B, Bompoint S, Heerspink HJL, Charytan DM, et al.: Canagliflozin and Renal Outcomes in Type 2 Diabetes and Nephropathy. *New England Journal of Medicine* 2019, 380:2295–2306.
[8] Heerspink HJL, Stefánsson BV, Correa-Rotter R, Chertow GM, Greene T, Hou F.-F, et al.: Dapagliflozin in Patients with Chronic Kidney Disease. *New England Journal of Medicine* 2020, 383:1436–1446.
[9] Sangeetha MK, Balaji Raghavendran HR, Gayathri V, Vasanthi HR: Tinospora Cordifolia Attenuates Oxidative Stress and Distorted Carbohydrate Metabolism in Experimentally Induced Type 2 Diabetes in Rats. *Journal of Natural Medicines* 2011, 65:544–550.
[10] Xie W, Du L: Diabetes is an Inflammatory Disease: Evidence from Traditional Chinese Medicines. *Diabetes, Obesity and Metabolism* 2011, 13:289–301.

[11] Ghosh D, Parida P: Drug Discovery and Development of Type 2 Diabetes Mellitus: Modern-Integrative Medicinal Approach. *Current Drug Discovery Technologies* 2016, 13:60–67.
[12] Phung OJ, Scholle JM, Talwar M, Coleman CI: Effect of Noninsulin Antidiabetic Drugs Added to Metformin Therapy on Glycemic Control, Weight Gain, and Hypoglycemia in Type 2 Diabetes. *Journal of the American Medical Association* 2010, 303:1410–1418.
[13] Zhu Y, Ouyang Z, Du H, Wang M, Wang J, Sun H, et al.: New Opportunities and Challenges of Natural Products Research: When Target Identification Meets Single-Cell Multiomics. *Acta Pharmaceutica Sinica B* 2022, 12:4011–4039.
[14] Kang NX, Zhu YJ, Zhao JP, Zhu WF, Liu YL, Xu QM, et al.: Antischistosomal Activity of Hederacochiside C against Schistosoma Japonicum Harbored in Experimentally Infected Animals. *Journal of Asian Natural Products Research* 2017, 19:402–415.
[15] Han S, Yuan R, Cui Y, He J, Wang QQ, Zhuo Y, et al.: Hederasaponin C Alleviates Lipopolysaccharide-Induced Acute Lung Injury *In Vivo* and *In Vitro* through the PIP2/NF-κB/NLRP3 Signaling Pathway. *Frontiers in Immunology* 2022, 13:846384.
[16] Zhou BC, Tian YG, Sun YN, Liu YL, Zhao D: A Validated LC-MS/MS Method for the Determination of Hederasaponin C: Application to Pharmacokinetics-Pharmacodynamics Studies in the Therapeutic Area of Acetic Acid-Induced Ulcerative Colitis in Rats. *Biomedical Chromatography* 2022, 36:e5450.
[17] Stuart T, Butler A, Hoffman P, Hafemeister C, Papalexi E, Mauck WM, et al.: Comprehensive Integration of Single-Cell Data. *Cell* 2019, 177:1888–1902.e21.
[18] Yu G, Wang LG, Han Y, He QY: clusterProfiler: An R Package for Comparing Biological Themes among Gene Clusters. *OMICS* 2012, 16:284–287.
[19] Hänzelmann S, Castelo R, Guinney J: GSVA: Gene Set Variation Analysis for Microarray and RNA-seq Data. *BMC Bioinformatics* 2013, 14:7.
[20] Ritchie ME, Phipson B, Wu D, Hu Y, Law CW, Shi W, et al.: limma Powers Differential Expression Analyses for RNA-Sequencing and Microarray Studies. *Nucleic Acids Research* 2015, 43:e47.
[21] Trapnell C, Cacchiarelli D, Grimsby J, Pokharel P, Li S, Morse M, et al.:The Dynamics and Regulators of Cell Fate Decisions are Revealed by Pseudotemporal Ordering of Single Cells. *Nature Biotechnology* 2014, 32:381–386.
[22] Shannon P, Markiel A, Ozier O, Baliga NS, Wang JT, Ramage D, et al.: Cytoscape: A Software Environment for Integrated Models of Biomolecular Interaction Networks. *Genome Research* 2003, 13:2498–2504.
[23] Teixeira SR, Tappenden KA, Erdman JW: Altering Dietary Protein Type and Quantity Reduces Urinary Albumin Excretion without Affecting Plasma Glucose Concentrations in BKS.cg-m +Lepr db/+Lepr db (db/db) Mice. *Journal of Nutrition* 2003, 133:673–678.
[24] Fan B, Li C, Szalad A, Wang L, Pan W, Zhang R, et al.: Mesenchymal Stromal Cell-Derived Exosomes Ameliorate Peripheral Neuropathy in a Mouse Model of Diabetes. *Diabetologia* 2020, 63:431–443.
[25] Pande M, Hur J, Hong Y, Backus C, Hayes JM, Oh SS, et al.: Transcriptional Profiling of Diabetic Neuropathy in the BKS db/db Mouse: A Model of Type 2 Diabetes. *Diabetes* 2011, 60:1981–1989.
[26] Guan J, Wang M, Zhao M, Ni W, Zhang M. Discovery of Fibrinogen γ-Chain as a Potential Urinary Biomarker for Renal Interstitial Fibrosis in IgA Nephropathy. BMC Nephrology. 2023, 24:60.
[27] Szklarczyk D, Gable AL, Nastou KC, Lyon D, Kirsch R, Pyysalo S, et al.: The STRING Database in 2021: Customizable Protein-Protein Networks, and Functional Characterization of User-Uploaded Gene/Measurement Sets. *Nucleic Acids Research* 2021, 49:D605–D612.
[28] Uehara-Watanabe N, Okuno-Ozeki N, Minamida A, Nakamura I, Nakata T, Nakai K, et al.: Direct Evidence of Proximal Tubular Proliferation in Early Diabetic Nephropathy. *Science Reports* 2022, 12:778.
[29] Ho KM, Morgan DJR: The Proximal Tubule as the Pathogenic and Therapeutic Target in Acute Kidney Injury. *Nephron* 2022, 146:494–502.
[30] Li S, Zhang Y, Lu R, Lv X, Lei Q, Tang D, et al.: Peroxiredoxin 1 Aggravates Acute Kidney Injury by Promoting Inflammation through Mincle/Syk/NF-κB Signaling. *Kidney International* 2023, 104:305–323.
[31] Higgins SP, Tang Y, Higgins CE, Mian B, Zhang W, Czekay RP, et al.: TGF-β1/p53 Signaling in Renal Fibrogenesis. *Cell Signal* 2018, 43:1–10.
[32] Aibar S, González-Blas CB, Moerman T, Huynh-Thu VA, Imrichova H, Hulselmans G, et al.: SCENIC: Single-Cell Regulatory Network Inference and Clustering. *Nature Methods* 2017, 14:1083–1086.
[33] Lin F, Zeng Z, Song Y, Li L, Wu Z, Zhang X, et al.: YBX-1 Mediated Sorting of miR-133 into Hypoxia/Reoxygenation-Induced EPC-Derived Exosomes to Increase Fibroblast Angiogenesis and MEndoT. *Stem Cell Research & Therapy* 2019, 10:263.
[34] Park J, Shrestha R, Qiu C, Kondo A, Huang S, Werth M, et al.: Single-Cell Transcriptomics of the Mouse Kidney Reveals Potential Cellular Targets of Kidney Disease. *Science* 2018, 360:758–763.
[35] Lindström NO, Guo J, Kim AD, Tran T, Guo Q, De Sena Brandine G, et al.: Conserved and Divergent Features of Mesenchymal Progenitor Cell Types within the Cortical Nephrogenic Niche of the Human and Mouse Kidney. *Journal of the American Society of Nephrology* 2018, 29:806–824.
[36] Wu H, Gonzalez Villalobos R, Yao X, Reilly D, Chen T, Rankin M, et al.: Mapping the Single-Cell Transcriptomic Response of Murine Diabetic Kidney Disease to Therapies. *Cell Metabolism* 2022, 34:1064–1078.e6.
[37] He B, Chen P, Zambrano S, Dabaghie D, Hu Y, Möller-Hackbarth K, et al.: Single-cell RNA Sequencing Reveals the Mesangial Identity and Species Diversity of Glomerular Cell Transcriptomes. *Nature Communications* 2021, 12:2141.
[38] Ning L, Suleiman HY, Miner JH: Synaptopodin Deficiency Exacerbates Kidney Disease in a Mouse Model of Alport Syndrome. *American Journal of Physiology-Renal Physiology* 2021, 321: F12–F25.
[39] Oleggini R, Bertelli R, Di Donato, A, Di Duca, M, Caridi G, Sanna-Cherchi S, et al.: Rare Functional Variants of Podocin (NPHS2) Promoter in Patients with Nephrotic Syndrome. *Gene Expression* 2006, 13:59–66.
[40] Zhao Y, Zou W, Du J, Zhao Y: The Origins and Homeostasis of Monocytes and Tissue-Resident Macrophages in Physiological Situation. *Journal of Cellular Physiology* 2018, 233:6425–6439.
[41] He Y, Deng B, Liu S, Luo S, Ning Y, Pan X, et al.: Myeloid *Piezo1* Deletion Protects Renal Fibrosis by Restraining

Macrophage Infiltration and Activation. *Hypertension* 2022, 79:918–931.

[42] Jere SW, Houreld NN, Abrahamse H: Role of the PI3K/AKT (mTOR and GSK3β) Signalling Pathway and Photobiomodulation in Diabetic Wound Healing. *Cytokine & Growth Factor Reviews* 2019, 50:52–59.

[43] Ou Y, Zhang W, Chen S, Deng H: Baicalin Improves Podocyte Injury in Rats with Diabetic Nephropathy by Inhibiting PI3K/Akt/mTOR Signaling Pathway. *Open Medicine (Warsaw)* 2021, 16:1286–1298.

[44] Jin S, Guerrero-Juarez CF, Zhang L, Chang I, Ramos R, Kuan CH, et al.: Inference and Analysis of Cell-Cell Communication using CellChat. *Nature Communications* 2021, 12:1088.

[45] Deng Y, Da J, Yu J, Zhou C, Yuan J, Zha Y: Single-Cell RNA Sequencing Data Analysis Suggests the Cell-Cell Interaction Patterns of the Pituitary-Kidney Axis. *Science Reports* 2022, 12:11147.

[46] Koutsioumpa M, Drosou G, Mikelis C, Theochari K, Vourtsis D, Katsoris P: Pleiotrophin Expression and Role in Physiological Angiogenesis In Vivo: Potential Involvement of Nucleolin. *Vascular Endothelial Cells* 2012, 4:4.

[47] Zhang T, Mo Q, Jiang N, Wu Y, Yang X, Chen W, et al.: The Combination of Machine Learning and Transcriptomics Reveals a Novel Megakaryopoiesis Inducer, MO-A, that Promotes Thrombopoiesis by Activating FGF1/FGFR1/PI3K/Akt/NF-κB Signaling. *European Journal of Pharmacology* 2023, 944:175604.

[48] Katoh M, Nakagama H: FGF Receptors: Cancer Biology and Therapeutics. *Medicinal Research Reviews* 2014, 34:280–300.

[49] Jiao J, Zhao X, Liang Y, Tang D, Pan C: FGF1-FGFR1 Axis Promotes Tongue Squamous Cell Carcinoma (TSCC) Metastasis through Epithelial-Mesenchymal Transition (EMT). *Biochemical and Biophysical Research Communications* 2015, 466:327–332.

[50] Liu Y: Cellular and Molecular Mechanisms of Renal Fibrosis. *Nature Reviews Nephrology* 2011, 7:684–696.

[51] Nogueira A, Pires MJ, Oliveira PA: Pathophysiological Mechanisms of Renal Fibrosis: A Review of Animal Models and Therapeutic Strategies. *In Vivo* 2017, 31:1–22.

[52] Zerbini G, Bonfanti R, Meschi F, Bognetti E, Paesano PL, Gianolli L, et al.: Persistent Renal Hypertrophy and Faster Decline of Glomerular Filtration Rate Precede the Development of Microalbuminuria in Type 1 Diabetes. *Diabetes* 2006, 55:2620–2625.

[53] Rigalleau V, Garcia M, Lasseur C, Laurent F, Montaudon M, Raffaitin C, et al.: Large Kidneys Predict Poor Renal Outcome in Subjects with Diabetes and Chronic Kidney Disease. *BMC Nephrology* 2010, 11:3.

[54] Humphreys BD: Mechanisms of Renal Fibrosis. *Annual Review of Physiology* 2018, 80:309–326.

[55] Wu M, Han W, Song S, Du Y, Liu C, Chen N, et al.: NLRP3 Deficiency Ameliorates Renal Inflammation and Fibrosis in Diabetic Mice. *Molecular and Cellular Endocrinology* 2018, 478:115–125.

[56] Qi R, Wang J, Jiang Y, Qiu Y, Xu M, Rong R, et al.: Snai1-Induced Partial Epithelial-Mesenchymal Transition Orchestrates p53-p21-Mediated G2/M Arrest in the Progression of Renal Fibrosis Via NF-κB-Mediated Inflammation. *Cell Death and Disease* 2021, 12:44.

[57] Iwano M, Plieth D, Danoff TM, Xue C, Okada H, Neilson EG: Evidence that Fibroblasts Derive from Epithelium during Tissue Fibrosis. *The Journal of Clinical Investigation* 2002, 110:341–350.

[58] Sun YB, Qu X, Caruana G, Li J: The Origin of Renal Fibroblasts/Myofibroblasts and the Signals that Trigger Fibrosis. *Differentiation* 2016, 92:102–107.

[59] Grande M, Sánchez-Laorden B, López-Blau C: Snail1-Induced Partial Epithelial-to-Mesenchymal Transition Drives Renal Fibrosis in Mice and can be Targeted to Reverse Established Disease. *Nature Medicine* 2015, 21:989–997.

[60] Rabb H, Griffin MD, McKay DB, Swaminathan S, Pickkers P, Rosner MH, et al.: Acute Dialysis Quality Initiative Consensus XIII Work Group: Inflammation in AKI: Current Understanding, Key Questions, and Knowledge Gaps. *Journal of the American Society of Nephrology* 2016, 27:371–379.

[61] Wang Y, Harris DC: Macrophages in Renal Disease. *Journal of the American Society of Nephrology* 2011, 22:21–27.

[62] You H, Gao T, Cooper TK, Brian Reeves W, Awad AS: Macrophages Directly Mediate Diabetic Renal Injury. *American Journal of Physiology-Renal Physiology* 2013, 305:F1719–F1727.

[63] Mortaz E, Alipoor SD, Adcock IM, Mumby S, Koenderman L: Update on Neutrophil Function in Severe Inflammation. *Frontiers in Immunology* 2018, 9:2171.

[64] Wang J: Neutrophils in Tissue Injury and Repair. *Cell Tissue Res* 2018, 371:531–539.

[65] Lin CJ, Chen TL, Tseng YY, Wu GJ, Hsieh MH, Lin YW, et al.: Honokiol Induces Autophagic Cell Death in Malignant Glioma through Reactive Oxygen Species-Mediated Regulation of the p53/PI3K/Akt/mTOR Signaling Pathway. *Toxicology and Applied Pharmacology* 2016, 304:59–69.

[66] Yalcin S, Marinkovic D, Mungamuri SK, Zhang X, Tong W, Sellers R, et al.: ROS-Mediated Amplification of AKT/mTOR Signalling Pathway Leads to Myeloproliferative Syndrome in Foxo3(–/–) Mice. *EMBO Journal* 2010, 29:4118–4131.

[67] Lamouille S, Derynck R: Emergence of the Phosphoinositide 3-Kinase-Akt-Mammalian Target of Rapamycin Axis in Transforming Growth Factor-β-Induced Epithelial-Mesenchymal Transition. *Cells Tissues Organs* 2011, 193:8–22.

[68] Roskoski R Jr: Vascular Endothelial Growth Factor (VEGF) and VEGF Receptor Inhibitors in the Treatment of Renal Cell Carcinomas. *Pharmacological Research* 2017, 120:116–132.

[69] Maheshwari A, Kelly DR, Nicola T, Ambalavanan N, Jain SK, Murphy-Ullrich J, et al.: TGF-β2 Suppresses Macrophage Cytokine Production and Mucosal Inflammatory Responses in the Developing Intestine. *Gastroenterology* 2011, 140:242–253.

[70] Zhang H, Yang P, Zhou H, Meng Q, Huang X: Involvement of Foxp3-Expressing CD4+ CD25+ Regulatory T Cells in the Development of Tolerance Induced by Transforming Growth Factor-Beta2-Treated Antigen-Presenting Cells. *Immunology* 2008, 124:304–314.

[71] Schenk S, Saberi M, Olefsky JM: Insulin Sensitivity: Modulation By Nutrients And Inflammation. *The Journal of Clinical Investigation* 2008, 118:2992–3002.

[72] Gifford CC, Tang J, Costello A, Khakoo NS, Nguyen TQ, Goldschmeding R, et al.: Negative Regulators of TGF-β1 Signaling in Renal Fibrosis; Pathological Mechanisms and Novel Therapeutic Opportunities. *Clinical Science (London)* 2021, 135:275–303.